Energetic Macroscopic Representation and Maximum Control Structure of Electric Vehicles Charging Photovoltaic System

Fabrice Locment, Manuela Sechilariu
AVENUES Team Research
University of Technology of Compiegne
Compiegne, France
fabrice.locment@utc.fr

Abstract—**Plug-in electric vehicles (EVs) can be fully or partially charged from a renewable energy source. In this paper a simulation model for an EVs charging system with photovoltaic grid-connected configuration is presented by using Energetic Macroscopic Representation (EMR) and Maximum Control Structure (MCS). The simulation results under different conditions show the validity of the model and the feasibility of the proposed system design.**

Keywords-modelling, simulation, EMR, MCS, photovoltaic, battery electric vehicle, public grid, control charging system.

I. INTRODUCTION

Plug-in electric hybrid vehicle (PHEV) and electric vehicle (EV) represent an important step in solving environmental problems and are being developed around the world. Many studies are going on to optimize engine and battery efficiency for both operations discharge and recharge. However, it is important to understand the further impact of PHEVs and mostly EVs recharging operation on the electric grid [1] [2]. Depending on when and where the vehicles are plugged in, they could cause strongly constraints on the grid. The expectation is that the grid will not be seriously affected because the recharging would mostly occur during the night hours. Nevertheless, the end-users preference to plug in when convenient for them, rather than utility grid would prefer, may be stronger. One of the solutions, from the environmental standpoint, is that the PHEVs and EVs can be fully or partially charged from a renewable energy source [3] [4]. Today, green energy purchase conditions lead quite naturally these applications to a grid-connected system with a total and permanent energy injection.

One of the largest French photovoltaic (PV) power plants grid-connected, designed by SUNVIE Company, is integrated into car parking shading over 800 spots, as shown on the Fig. 1. It is matter of 5,472 CONERGY S210 PV panels (1.15MW_P on 8045m^2) which whole electricity production is sold back into the grid, by means of two inverters SMA, 0.5MW each. This car parking transformed into PV power plant operates an area otherwise unused to produce renewable electricity and provides sun car protection needed during the summer season. It is a real green built environment. However, tomorrow most cars will be electric, and thus recharging their batteries will be a real need. In this case, the EVs will be recharged directly on the grid by using specific rectifiers. So, two problems arise: grid availability to enable recharging and global energy efficiency recharging using the AC-DC energy conversion. Having regard to the absence of ancillary services of PV grid-connected system and to above-mentioned technical constraints, this development could be restrained. In this context, PV power stations associated or integrated with car parking and recharging stations that allows the EVs charging directly from the PV power and a bidirectional energy flow from/to the grid is an alternative solution to those technical difficulties. This system is a PV power local generation, whose energy produced is intended priority for self-feeding, with a grid connection for further supply in case of need and for sale of excess energy.

This paper focuses on a global energetic modelling that uses Energetic Macroscopic Representations (EMR) of a PV grid-connected system, which allows the EVs feeding at the same time as PV energy production. Different energetic configurations of the available power and energy sources are presented. Then, the Maximum Control Structure (MCS) deduced from the EMR is given and simulation results performed with MATLAB Simulink are presented and discussed.

Figure 1. Car parking sheds with photovoltaic power plant.

978-1-4244-8218-4/10/$26.00 ©2010 IEEE

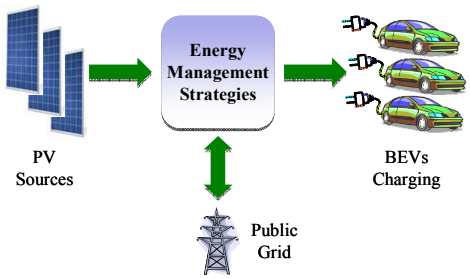

Figure 2. EVs charging station with PV grid-connected system.

II. ELECTRIC VEHICLES CHARGING STATION

Many PV power stations operate in a grid-connected mode, which involves no interaction with a load. The proposed system allows both connections, with set of battery electric vehicle (BEV), as load, and public grid.

A. General System Overview

The EVs charging system with PV grid-connected configuration is presented on the Fig. 2. It is a matter of PV local power generation with an integrated energy management system operating under the assumption that the locally generated power is used where, when, and how it is generated; the public grid is used only as a backup and if available. That could eliminate energy consumption from the public grid by means of self-feeding and sale the excess power only. When the sunshine is too weak to generate the entire necessary power to transfer to the BEVs, the public grid supplies the DC load also. In contrast, when the generated PV power is more important than the BEVs demanded power, the system sends power back to the grid. The bidirectional energy flow from/to the grid is operated taking into account the public grid availability.

B. Electrical system description

The EVs charging plant, illustrated on the Fig. 3, consists of public grid electrically coupled via a transformer and line inductors to two identical systems. Each system, n-indexed $n \in \{1,2\}$, is composed by: inverter (0.5MW) with the following switching functions f_{A_n}, f_{B_n}, f_{C_n}, PV installation (PV_n), power converter leg with f_{L_n} switching function, BEV load (L_n). Switching functions are equal to 0 or 1. Inductors and capacitors are used in order to ensure compatibility between the different elements. The principal subsystems are: PV sources, public grid, BEVs charging.

III. ENERGETIC MACROSCOPIC REPRESENTATION

EMR is a synthetic graphic tool that uses causal or functional modelling. It allows studying in a systematic way all the interactions between the different subsystems of a complex system. The elements of the system are represented by pictograms (see Appendix); they are interconnected following the action reaction principle and respecting the integral causality. Each pictogram is internally described using transfer functions, mathematical relations or another modelling tool. The instantaneous exchanged power is the product between action and reaction variables, represented by arrows (inputs and outputs). EMR has several advantages: it allows the representation of multi physics systems, the systematic deduction of control structures, and the implementation is usually performed on MATLAB Simulink. The EMR formalism has been already used in many real applications [5] [6] [7] [8].

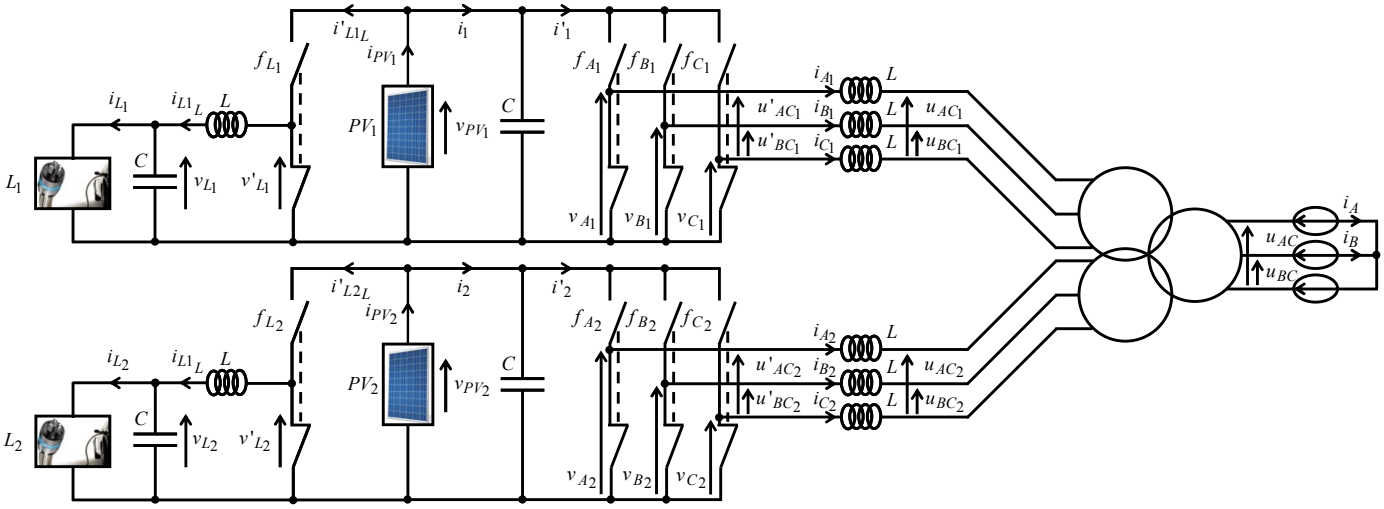

Figure 3. Electrical scheme of EVs charging station with PV grid-connected system.

A. EMR of PV sources subsystem

The simulation study aims to approach the technical data from the installation SUNVIE presented in introduction, in particular the maximum power of PV sources. However, experimental testing of electrical characterization has been done in our laboratory for PV panel Solar-Fabrik SF-130/2-125 (Fig. 4). Therefore, it is taken into account for 12 sunshades 9,408 PV panels and 1.176MW$_P$, each sunshade with 14 PV strings and 56 PV panels by string (in order not to exceed the permissible maximum voltage by PV). Thus, each PV source of 588kW$_P$ refers mainly to 4,704 PV panels (SF-130/2-125).

The PV_n is modelled as a source power which imposes the current i_{PV_n} and recovers the voltage v_{PV_n}.

B. EMR of public grid subsystem

PV sources are electrically connected to inverters by capacitors (C). This electrically coupling is modelled by (1).

$$\frac{dv_{PV_n}}{dt} = \frac{i_{PV_n} - i'_{Ln_L} - i'_n}{C} \tag{1}$$

In order to design EMR of inverters, the simple voltages of the three phases and corresponding inverter switching functions (f_{A_n} , f_{B_n} , f_{C_n}) are used as shown by (2):

$$\begin{bmatrix} u'_{AC_n} \\ u'_{BC_n} \end{bmatrix} = \begin{bmatrix} v_{A_n} - v_{C_n} \\ v_{B_n} - v_{C_n} \end{bmatrix} \; ; \; \begin{bmatrix} v_{A_n} \\ v_{B_n} \\ v_{C_n} \end{bmatrix} = \begin{bmatrix} f_{A_n} \\ f_{B_n} \\ f_{C_n} \end{bmatrix} v_{PV_n}$$

$$\begin{bmatrix} v_{A_n} \\ v_{B_n} \\ v_{C_n} \end{bmatrix} = \begin{bmatrix} f_{A_n} - f_{C_n} \\ f_{B_n} - f_{C_n} \end{bmatrix} v_{PV_n} \Rightarrow \begin{bmatrix} v_{A_n} \\ v_{B_n} \\ v_{C_n} \end{bmatrix} = \begin{bmatrix} m_{A_n} \\ m_{B_n} \end{bmatrix} v_{PV_n} \tag{2}$$

$$\begin{bmatrix} m_{A_n} \\ m_{B_n} \end{bmatrix} = \frac{1}{T}\int_0^T \begin{bmatrix} f_{A_n} - f_{C_n} \\ f_{B_n} - f_{C_n} \end{bmatrix} dt \text{ with } \begin{bmatrix} m_{A_n} \\ m_{B_n} \end{bmatrix} \in [-1;1]$$

The currents are expressed by (3).

$$\begin{aligned} i'_n &= f_{A_n} i_{A_n} + f_{B_n} i_{B_n} + f_{C_n} i_{C_n} \text{ with } i_{A_n} + i_{B_n} + i_{C_n} = 0 \\ i'_n &= \left(f_{A_n} - f_{C_n}\right) i_{A_n} + \left(f_{B_n} - f_{C_n}\right) i_{B_n} = m_{A_n} i_{A_n} + m_{B_n} i_{B_n} \end{aligned} \tag{3}$$

The connection between inverters and transformer is carried out by power lines, which no mutual each inductor has an inductance L and an internal resistance R . The relationship between voltages and currents of power lines is given in (4):

$$\begin{bmatrix} u'_{AC_n} \\ u'_{BC_n} \end{bmatrix} - \begin{bmatrix} u_{AC_n} \\ u_{BC_n} \end{bmatrix} = \begin{bmatrix} 2L & L \\ L & 2L \end{bmatrix} \frac{d}{dt} \begin{bmatrix} i_{A_n} \\ i_{B_n} \end{bmatrix} + \begin{bmatrix} 2R & R \\ R & 2R \end{bmatrix} \begin{bmatrix} i_{A_n} \\ i_{B_n} \end{bmatrix} \tag{4}$$

The public grid (PG) is a 20kV phase-to-phase network ($u_{AC} = u_{BC} = 20\text{kV}$). It is connected to both inverters via a transformer and power lines. The transformer has a transformation ratio k equal to 0.02 (transformer used is assumed to be perfect), which provides a voltage of 400V phase to phase ($u_{AC_1} = u_{BC_1} = u_{AC_2} = u_{BC_2} = 400\text{V}$).

$$\begin{bmatrix} u_{AC_n} \\ u_{BC_n} \end{bmatrix} = k \begin{bmatrix} u_{AC} \\ u_{BC} \end{bmatrix}$$
$$k \begin{bmatrix} i_{A_1} + i_{A_2} \\ i_{B_1} + i_{B_2} \end{bmatrix} = \begin{bmatrix} i_A \\ i_B \end{bmatrix} \tag{5}$$

C. EMR of BEVs charging subsystem

It is assumed that vehicles connecting to this system are equipped with Li-ion battery. The Li-ion battery is assumed to be charged with a so-called CC/CV procedure [9]. This one consists to charge a Li-ion battery in two modes, a constant current (CC) mode followed by a constant voltage (CV) mode. During the CC mode, the charging current stays constant until the voltage rises to a cut-off voltage. In our case, this voltage is 3.6V per cell. It is supposed that all the cells of the battery pack are balanced by a battery management system. During the CV mode, the voltage remains constant while the current drops. A CC/CV procedure has been applied to an A123 LiFePO4 26650 cell and recorded. In order to emulate the BEV charging, we have considered a CC/CV profile proportional to the profile recorded on one cell. Fig. 5 shows power and battery state of charge (SOC) of one vehicle. These characteristics are obtained by coupling 28 parallel branches of 120 serial cells. The whole charge is near 24kWh energy stored.

The electricity demand varied strongly. That depends on type of vehicle, its battery SOC, charge voltage and current level and charging duration.

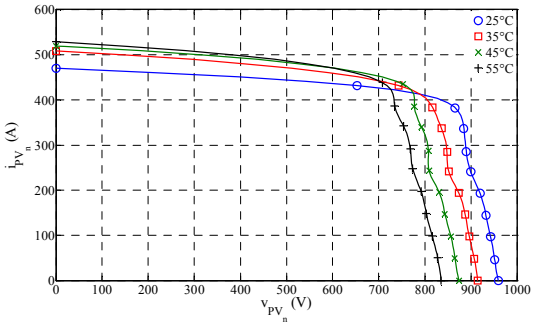

Figure 4. Experimental voltage and current for one PV source for 600W/m2.

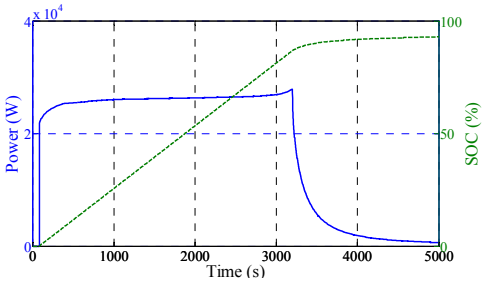

Figure 5. BEV charge profile.

In this work, for each vehicle, the described BEV charging system is assumed. The system imposes a constant DC voltage. The following chopper carries out BEV correctly charging:

$$\begin{aligned} v'_{L_n} &= f_{L_n}\, v_{PV_n} = m_{L_n}\, v_{PV_n} \\ i'_{Ln_L} &= f_{L_n}\, i_{L_n} = m_{L_n}\, i_{L_n} \\ m_{L_n} &= \frac{1}{T}\int_0^T f_{L_n}\, dt \text{ with } m_{L_n} \in [0;1] \\ \frac{di_{Ln_L}}{dt} &= \frac{v'_{L_n} - v_{L_n}}{L} \\ \frac{dv_{L_n}}{dt} &= \frac{i_{Ln_L} - i_{L_n}}{C} \end{aligned} \tag{6}$$

Arbitrarily, it was decided that 20 vehicles could be recharged simultaneously by PV_n. Thus, BEVs' power supply should not exceed the PV maximum power. Furthermore, it is assumed that, for all BEVs, charging starts from zero SOC limit and all plug-in vehicles remain for the entire CC/CV procedure. Fig. 6 shows vehicles' number evolution and corresponding absorbed power ($p_{L_n} = v_{L_n}\, i_{L_n}$).

Starting from each EMR subsystem, the global EMR of EVs charging station with PV grid-connected system is obtained and shown on the Fig. 7. This system has five state variables (v_{L_n} , i_{Ln_L} , v_{PV_n} , i_{A_n} and i_{B_n}) and three control variables (m_{L_n} , m_{A_n} and m_{B_n}). A control strategy according to the running system is needed.

IV. MAXIMUM CONTROL STRUCTURE

EMR formalism is helpful to design control structures. Thus, a corresponding Maximum Control Structure (MCS) is deduced from the EMR described earlier, through specific inversion rules: direct inversion (without controller) for items that are not time function, indirect inversion (with controller) for items that are time function.

The control variable m_{L_n} imposes a constant DC voltage (v_{L_n}) across the terminals of the vehicles. Using the above mentioned specific inversion rules it is obtained:

$$\begin{aligned} v'^{*}_{L_n} &= C_L\left(i^{*}_{Ln_L} - i_{Ln_L}\right) + v_{L_n} \text{ with} \\ i^{*}_{Ln_L} &= C_C\left(v^{*}_{L_n} - v_{L_n}\right) + i_{L_n} \\ m^{*}_{L_n} &= \frac{v'^{*}_{L_n}}{v_{PV_n}} = \frac{\left(C_L\left(C_C\left(v^{*}_{L_n} - v_{L_n}\right) + i_{L_n} - i_{Ln_L}\right) + v_{L_n}\right)}{v_{PV_n}} \end{aligned} \tag{7}$$

C_L is proportional integral corrector with a bandwidth of 500Hz. It has been defined by the method of the dominant pole compensation. C_C is proportional corrector with a bandwidth of 50Hz.

The control variables m_{A_n} and m_{B_n} imposes a variable DC voltage (v_{PV_n}) across the terminals of PV sources. Value of this reference voltage ($v^{*}_{PV_n}$) is imposed by an MPPT algorithm. In this work, "Perturb & Observe" (P&O) algorithm is used to extract the maximum power of PV for any value of solar irradiance and temperature. The P&O method claimed by many in the literature to be inferior to others continue to be by far the most widely used method in commercial PV panel because it is easy to implement [10].

Inverting (1) allows obtaining (8)

$$i'^{*}_{n} = -C_C\left(v^{*}_{PV_n} - v_{PV_n}\right) + i_{PV_n} - i'_{Ln_L} \tag{8}$$

Performing a power balance and assuming that the switches are ideal, the active power reference, modelled on two-phase alpha-beta frame, is equal to:

$$p^{*}_{n} = v_{\alpha_n} i^{*}_{\alpha_n} + v_{\beta_n} i^{*}_{\beta_n} = v_{PV_n}\, i'^{*}_{n} \tag{9}$$

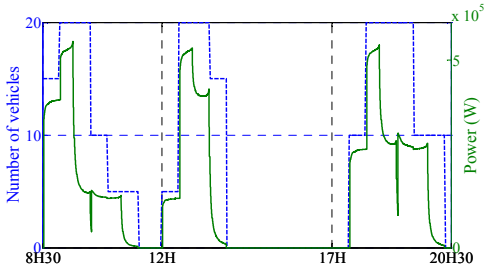

Figure 6. Vehicles' number evolution and corresponding absorbed power.

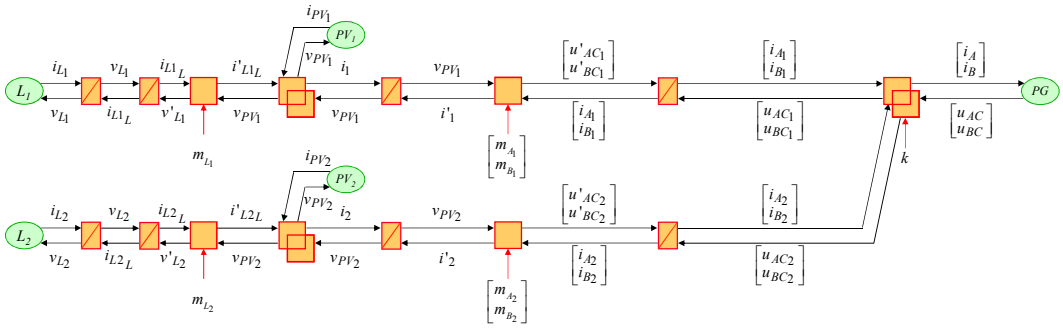

Figure 7. EMR of EVs charging station with PV grid-connected system.

with:

$$\begin{bmatrix} v_{\alpha_n} \\ v_{\beta_n} \end{bmatrix} = [T] \begin{bmatrix} v_{A_n} \\ v_{B_n} \\ v_{C_n} \end{bmatrix} = \sqrt{\frac{2}{3}} \begin{bmatrix} 1 & -\frac{1}{2} & -\frac{1}{2} \\ 0 & \frac{\sqrt{3}}{2} & -\frac{\sqrt{3}}{2} \end{bmatrix} \begin{bmatrix} v_{A_n} \\ v_{B_n} \\ v_{C_n} \end{bmatrix}$$
$$\begin{bmatrix} i_{\alpha_n} \\ i_{\beta_n} \end{bmatrix} = [T] \begin{bmatrix} i_{A_n} \\ i_{B_n} \\ i_{C_n} \end{bmatrix} = \sqrt{\frac{2}{3}} \begin{bmatrix} 1 & -\frac{1}{2} & -\frac{1}{2} \\ 0 & \frac{\sqrt{3}}{2} & -\frac{\sqrt{3}}{2} \end{bmatrix} \begin{bmatrix} i_{A_n} \\ i_{B_n} \\ i_{C_n} \end{bmatrix} \quad (10)$$

The reactive power reference is imposed arbitrarily to zero and is defined by:

$$q_n^* = v_{\alpha_n} i_{\beta_n}^* - v_{\beta_n} i_{\alpha_n}^* = 0 \quad (11)$$

From (9) and (10) the current references ($i_{\alpha_n}^*$, $i_{\beta_n}^*$) can be determined:

$$i_{\alpha_n}^* = \frac{v_{\alpha_n} p_n^* - v_{\beta_n} q_n^*}{v_{\alpha_n}^2 + v_{\beta_n}^2}$$
$$i_{\beta_n}^* = \frac{v_{\beta_n} p_n^* + v_{\alpha_n} q_n^*}{v_{\alpha_n}^2 + v_{\beta_n}^2} \quad (12)$$

In order to simplify the control currents, regulation is performed in dq reference frame using the following transition matrix:

$$\begin{bmatrix} i_{d_n}^* \\ i_{q_n}^* \end{bmatrix} = [R(\theta)] \begin{bmatrix} i_{\alpha_n}^* \\ i_{\beta_n}^* \end{bmatrix} = \begin{bmatrix} \cos(\theta) & -\sin(\theta) \\ \sin(\theta) & \cos(\theta) \end{bmatrix} \begin{bmatrix} i_{\alpha_n}^* \\ i_{\beta_n}^* \end{bmatrix} \quad (13)$$

where θ is the phase shift between the voltages and currents.

The current references are known, therefore it is possible to determine the expression of the control variables m_{A_n} and m_{B_n}:

$$\begin{bmatrix} m_{A_n}^* \\ m_{B_n}^* \end{bmatrix} = \frac{1}{v_{PV_n}} [T]^{-1} \left([R(\theta)]^{-1} \left(C_L \begin{bmatrix} i_{d_n}^* - i_{d_n} \\ i_{q_n}^* - i_{q_n} \end{bmatrix} \right) + \begin{bmatrix} v_{\alpha_n} \\ v_{\beta_n} \end{bmatrix} \right) \quad (14)$$

The EMR allows developing rapidly the system's MCS. Fig. 8 presents the MCS of EV charging PV grid-connected system. This graphical description gives particularly the P&O strategy, symbolized by S, and the secure operating system.

V. Simulation Results

The main objective of this work was to validate a comprehensive approach, rather purely numerical results. Before obtaining the overall studied system simulation results, which were performed with MATLAB Simulink, each subsystem was validated. The simulation results were obtained with the following values: $v_{L_n}^* = 500\text{V}$, $C = 10\text{mF}$ and $L = 1\text{mH}$ (with $1\text{m}\Omega$ internal resistance). The calculation step is 5kHz. The most important powers in this simulation are: $p_{PV_n} = v_{PV_n}\, i_{PV_n}$ power supplied by PV_n source, $p_{L_n} = v_{L_n}\, i_{L_n}$ power requested by BEVs, p_n public grid active power transfer.

Fig. 9 gives the solar irradiance and PV cell temperature during the day of November 20th, 2009 at Compiegne, France. Fig. 10 shows the evolution of voltage v_{PV_n} and reference voltage $v_{PV_n}^*$; these settings evolutions are almost the same. Fig. 9 and Fig. 10 prove that the P&O algorithm work correctly according to v_{PV_n} proportional to solar irradiance evolution.

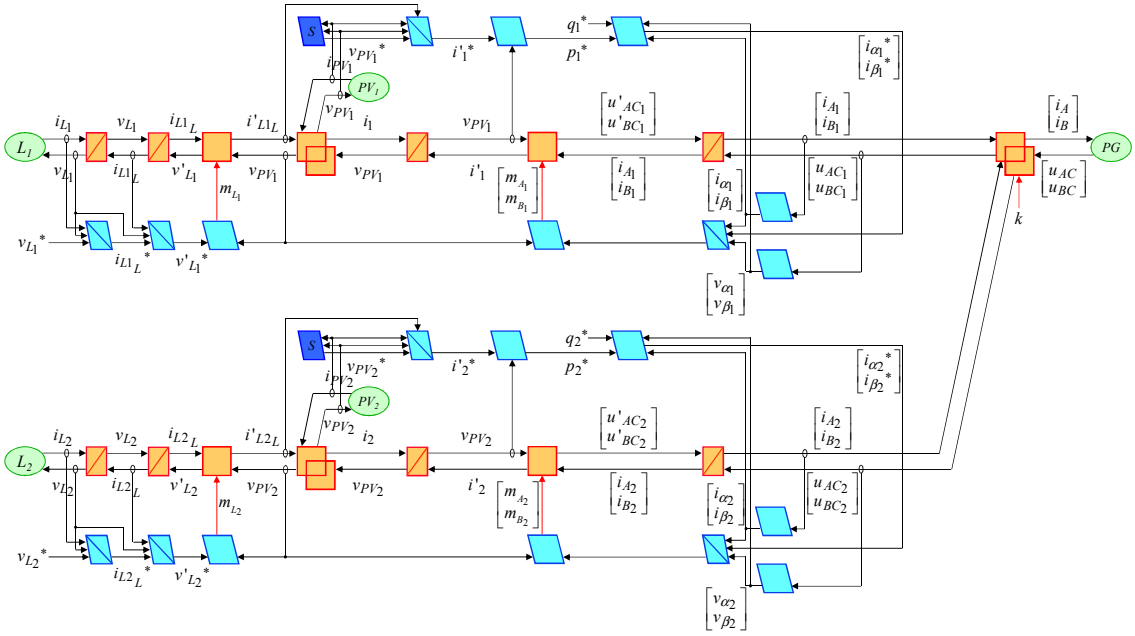

Figure 8. MCS of EVs charging station with PV grid-connected system.

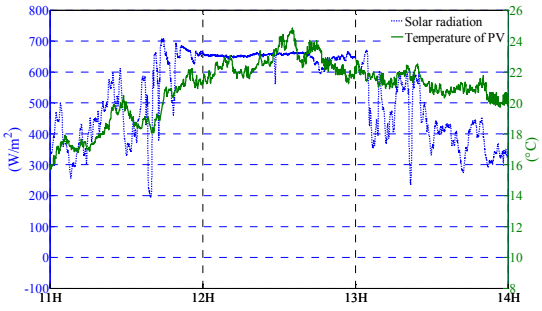

Figure 9. Solar irradiance and PV cell temperature on November 20th, 2010.

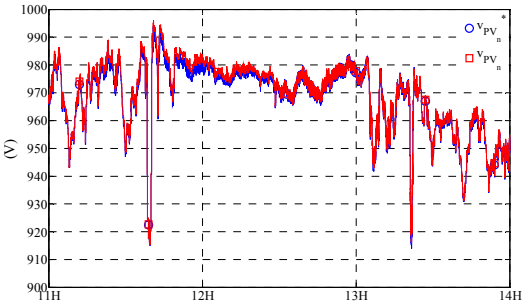

Figure 10. Evolution of PV_n voltages following P&O MPPT algorithm.

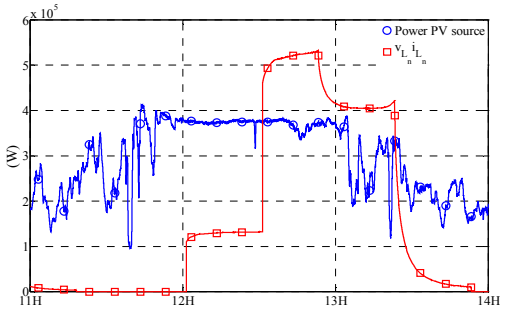

Figure 11. Power supplied by PV_n source and power absorbed by corresponding BEVs.

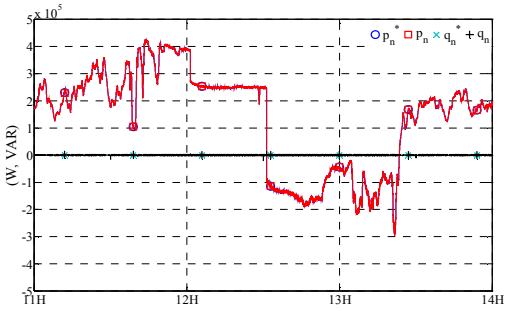

Figure 12. Public grid active and reactive powers evolution.

Fig. 11 and Fig. 12 show EV charging PV grid-connected system's powers evolution. For the period taken into account, we observe that the strategy outlined earlier is well respected at all times.The PV energy produced remains priority for self-feeding. In case of insufficient energy toward BEVs the system security is ensured thanks to the grid connection.

Thus, for $p_{PV_n} > p_{L_n}$ the public grid receives energy, in contrast it provides. These results show that whatever the sign and the amplitude of the difference of power between p_{PV_n} and p_{L_n} this experimental system is secured.

VI. CONCLUSION

In this paper, the model of an EVs charging system with PV grid-connected configuration was built by using EMR. The system has been simulated using the corresponding MCS deduced from the EMR, and implemented in MATLAB Simulink. This formalism is useful for studying the different control and energy management strategies. The simulation results show the feasibility of the system design that permits a lesser impact with the grid and improves the energy efficiency of BEVs recharging.

ACKNOWLEDGMENT

The authors of the article thank SUNVIE Company for the transmission of the technical data on parking shopping center PV power plant of Saint-Aunès, France.

REFERENCES

[1] S. D. Jenkins, J. R. Rossmaier, and M. Ferdowsi, "Utilization and effect of plug-in hybrid electric vehicles in the United States power grid", IEEE Vehicle Power and Propulsion Conference 2008, VPPC 08, 3-5 Sept. 2008, page(s): 1-5.

[2] EPRI, "Environmental Assessment of Plug-In Hybrid Electric Vehicles; Volume 1: Nationwide Greenhouse Gas Emissions", Final Report, July 2007.

[3] V. Marano and G. Rizzoni, "Energy and Economic Evaluation of PHEVs and their Interaction with Renewable Energy Sources and the Power Grid", IEEE International Conference on Vehicular Electronics and Safety Columbus, 2008.

[4] X. Li, L. A. C. Lopes, and S. S. Williamson, "On the suitability of plug-in hybrid electric vehicle (PHEV) charging infrastructures based on wind and solar energy", IEEE Power & Energy Society General Meeting, PES 2009.

[5] P. Delarue, A. Bouscayrol, A. Tounzi, X. Guillaud, and G. Lancigu, "Modelling, control and simulation of an overall wind energy conversion system", Renewable Energy, vol. 28, no. 8, July 2003, page(s): 1169-1185.

[6] A. Bouscayrol, M. Pietrzak-David, P. Delarue, R. Pena-Eguiluz, P. E. Vidal and X. Kestelyn, "Weighted Control of Traction Drives With Parallel-Connected AC Machines", IEEE Transactions on Industrial Electronics, Vol 53, Issue 6, Dec. 2006, page(s):1799 – 1806.

[7] K. Chen, A. Bouscayrol, A. Berthon, P. Delarue, D. Hissel and R. Trigui. Global modeling of different vehicles using energetic macroscopic representation, IEEE Vehicle Power and Propulsion Conference 2008, VPPC 08, 3-5 Sept. 2008, page(s): 1-7.

[8] H. Yu, R. Lu, T. Wang, and C. Zhu, "Energetic Macroscopic Representation Based Modeling and Control for Battery/Ultra-capacitor Hybrid Energy Strorage System in HEV", IEEE Vehicle Power and Propulsion Conference 2009, VPPC 09, 7-10 Sept. 2009, page(s): 1390-1394.

[9] H. J. Bergveld, P. H. L. Notten and W. S. Kruijt, "Battery management systems: design by modeling", Kluwer Academic Publishers, 2002.

[10] I. Houssamo, F. Locment and M. Sechilariu, "Maximum power tracking for photovoltaic power system: Development and experimental comparison of two algorithms", Renewable Energy 35-10, 2010, page(s): 2381-2387.